Contents lists available at ScienceDirect

Chemical Engineering Research and Design

journal homepage: www.elsevier.com/locate/cherd

Real-time machine learning for operational safety of nonlinear processes via barrier-function based predictive control

Zhe Wu[a], *David Rincon*[a], *Panagiotis D. Christofides*[a,b,*]

[a] *Department of Chemical and Biomolecular Engineering, University of California, Los Angeles, CA 90095-1592, USA*
[b] *Department of Electrical and Computer Engineering, University of California, Los Angeles, CA 90095-1592, USA*

ARTICLE INFO

Article history:
Received 4 December 2019
Received in revised form 28 December 2019
Accepted 3 January 2020
Available online 10 January 2020

Keywords:
Machine learning
Model predictive control
Control Lyapunov–barrier functions
Nonlinear systems
Chemical processes

ABSTRACT

This work proposes a real-time model predictive control (MPC) system using control Lyapunov–barrier functions (CLBF) and recurrent neural network (RNN) models to ensure simultaneous closed-loop stability and operational safety for a general class of nonlinear systems subject to time-varying disturbances. An RNN model is first developed for the nominal system (i.e., without disturbances) and incorporated in the designs of CLBF-based MPC and of CLBF-based economic MPC (EMPC) to provide state predictions for the optimization problems of MPCs. Subsequently, to improve the closed-loop performance in terms of operational safety and stability in the presence of disturbances, online learning of RNN models is incorporated within the real-time implementation of CLBF-MPC and of CLBF-EMPC to update the RNN models using the most recent process measurement data. The proposed adaptive machine-learning-based CLBF-MPC and CLBF-EMPC schemes are evaluated using a nonlinear chemical process example.

1. Introduction

Recurrent neural networks (RNN) have demonstrated their capability in approximating complex, nonlinear dynamic systems in the discipline of data-driven modeling, (e.g., You and Nikolaou, 1993; Kosmatopoulos et al., 1995; Trischler and D'Eleuterio, 2016). As RNNs are able to capture temporal dynamic behavior via the feedback loops that bring past neuron information into the current network, they have been utilized to construct dynamic process models for model-based optimization of chemical processes when a first-principles model is unavailable. For example, RNN modeling methods have been recently incorporated in the design of model predictive control (MPC) to operate a nonlinear process at the steady-state while optimizing process dynamic performance. In Wu et al. (2019c), it is demonstrated that the desired closed-loop performance in terms of guaranteed stability, optimal response, and smooth control actions can be achieved under the MPC using an ensemble of RNN models that well capture process nonlinear dynamics. In Wong et al. (2018), RNN models were utilized to provide a dynamic process model for MPC to operate a continuous reactor for pharmaceutical manufacturing. In addition to process stability, another issue that is of significant importance in chemical process operation and has attracted a lot of attention in the engineering community is process operational safety. To ensure that a process is being operated in safe operating conditions for all times, safety protection systems including process control systems, alarms systems and emergency shutdown systems have been developed and widely-used in industry. Specifically, advanced process control systems at the lowest level of safety protection system need to be designed to account for safety consid-

* *Corresponding author at*: Department of Chemical and Biomolecular Engineering, University of California, Los Angeles, CA 90095-1592, USA
E-mail address: pdc@seas.ucla.edu (P.D. Christofides).
https://doi.org/10.1016/j.cherd.2020.01.007

erations such as operating the system safely and avoiding triggering alarms systems too frequently.

To that end, control Lyapunov–barrier functions (CLBF) (Romdlony and Jayawardhana, 2016) that are designed based on control Lyapunov functions and control barrier functions (Ames et al., 2016; Jankovic, 2017) have been utilized to design the safety constraints for MPC to stabilize the closed-loop state at its steady-state and avoid unsafe operating regions in state-space. It has been demonstrated in Wu et al. (2019a) that under CLBF-MPC, closed-loop stability and process operational safety can be achieved for nonlinear processes with guaranteed recursive feasibility of the optimization problem of CLBF-MPC. Additionally, in Wu and Christofides (2019b), CLBF-based constraints are incorporated in the design of machine learning-based EMPC to achieve process operational safety and economic optimality simultaneously by dynamically operating the system in a stability region.

Despite the successful applications of machine-learning-based controllers for closed-loop stability and process operational safety, there is an increasing need to address online learning of machine learning models as all real-world processes are changing over time due to external disturbances and internal variations (e.g., catalyst deactivation) (Valappil and Georgakis, 2000; Marquardt, 2002). For example, an event-triggered feedback system was design in Wang and Lemmon (2008) to stabilize a nonlinear system by updating control actions when the stability condition is violated. Additionally, the event-triggered mechanism has also been incorporated in the design of neural network-based control schemes in Sahoo et al. (2015), Liu and Yang (2018), Wu et al. (2019b). For example, adaptive machine-learning-based MPC has been developed in Wu et al. (2019b) to improve closed-loop performances by updating RNN models using real-time process data for nonlinear processes subject to time-varying disturbances.

Motivated by the above, in this work, we develop a real-time adaptive CLBF-based MPC scheme that updates RNN models following the event-triggered and error-triggered mechanisms that have been proposed in Wu et al. (2019b). Specifically, an RNN-based CLBF-MPC and an RNN-based CLBF-EMPC are first developed following Wu et al. (2019a) and Wu and Christofides (2019b) to derive closed-loop stability and safety for the nominal system. Subsequently, online learning of RNN models is incorporated in the real-time implementation of CLBF-MPC and of CLBF-EMPC to adapt the RNN models to time-varying disturbances such that the system can be operated safely in the sense that the closed-loop state can be driven to its steady-state under CLBF-MPC, and can be maintained in the stability region under CLBF-EMPC, while avoiding the unsafe region in state-space in the presence of disturbances. Finally, the real-time machine learning-based CLBF-MPC and CLBF-EMPC are applied to a chemical process example to demonstrate their improved closed-loop performances compared to those under the CLBF-MPC and CLBF-EMPC without online learning of RNN models.

2. Preliminaries

2.1. Notation

The notation $|\cdot|$ is used to denote the Euclidean norm of a vector. x^T denotes the transpose of x. The notation $L_f V(x)$ denotes the standard Lie derivative $L_f V(x) := \frac{\partial V(x)}{\partial x} f(x)$. Set subtraction is denoted by "\", i.e., $A \backslash B := \{x \in \mathbf{R}^n | x \in A, x \notin B\}$. $\emptyset$ signifies the empty set. The function $f(\cdot)$ is of class $\mathcal{C}^1$ if it is continuously differentiable in its domain. A continuous function $\alpha : [0, a) \to [0, \infty)$ is said to belong to class $\mathcal{K}$ if it is strictly increasing and is zero only when evaluated at zero.

2.2. Class of systems

The class of continuous-time nonlinear systems considered is described by the first-order nonlinear ordinary differential equations (ODEs) as follows:

$$\dot{x} = f(x) + g(x)u + h(x)w, \quad x(t_0) = x_0 \tag{1}$$

where $x \in \mathbf{R}^n$ is the state vector, $u \in \mathbf{R}^m$ is the manipulated input vector, and $w \in W$ is the disturbance vector bounded by $W := \{w \in \mathbf{R}^q | |w| \leq w_m, w_m \geq 0\}$. The control action constraint is defined by $u \in U := \{u_i^{\min} \leq u_i \leq u_i^{\max}, i = 1, \ldots, m\} \subset \mathbf{R}^m$. $f(\cdot)$, $g(\cdot)$ and $h(\cdot)$ are sufficiently smooth vector and matrix functions of dimensions $n \times 1$, $n \times m$, and $n \times q$, respectively. Throughout the manuscript, the initial time t_0 is taken to be zero ($t_0 = 0$), and it is assumed that $f(0) = 0$, and thus, the origin is a steady-state of the nominal system of Eq. (1) with $w(t) \equiv 0$, (i.e., $(x_s^*, u_s^*) = (0, 0)$).

2.3. Stabilizability assumptions and safety considerations

A positive definite control Lyapunov function (CLF) V that satisfies the small control property (i.e., for every $\varepsilon > 0$, $\exists \delta > 0$, s.t. $\forall x \in \mathcal{B}_\delta(0)$, there exists u that satisfies $|u| < \varepsilon$ and $L_f V(x) + L_g V(x) u < 0$, Sontag, 1989) and the following condition is assumed to exist for the nominal system of Eq. (1) with $w(t) \equiv 0$:

$$L_f V(x) < 0, \quad \forall x \in \{z \in \mathbf{R}^n \backslash \{0\} | L_g V(z) = 0\} \tag{2}$$

The above CLF assumption implies that there exists a stabilizing feedback control law $\Phi(x) \in U$ for the nominal system of Eq. (1) (i.e., $w(t) \equiv 0$) that renders the origin of the closed-loop system asymptotically stable for all x in a neighborhood of the origin.

Additionally, we assume that there exists a set $\mathcal{D} \subset \mathbf{R}^n$ in state-space within which it is unsafe for the system to be operated, and a safe stability region $\mathcal{U}$ such that $\mathcal{U} \cap \mathcal{D} = \emptyset$ and $\{0\} \subset \mathcal{U}$, within which closed-loop stability and process operational safety are achieved simultaneously in the following sense:

Definition 1. Wu and Christofides (2019a) Consider the system of Eq. (1) and input constraints $u \in U$. If there exists a control law $u = \Phi(x) \in U$ such that for any initial state $x(t_0) = x_0 \in \mathcal{U}$, $x(t)$ remains inside $\mathcal{U}$, $\forall t \geq 0$, and the origin of the closed-loop system of Eq. (1) can be rendered asymptotically stable, we say that the control law $\Phi(x)$ maintains the process state within a safe stability region $\mathcal{U}$ at all times.

2.4. Recurrent neural network

The following recurrent neural network (RNN) model is developed to approximate the nonlinear dynamics of the system of Eq. (1):

$$\dot{\hat{x}} = F_{nn}(\hat{x}, u) := A\hat{x} + \Theta^T y \tag{3}$$

where $\hat{x} \in \mathbf{R}^n$ is the RNN state vector and $u \in \mathbf{R}^m$ is the manipulated input vector. $y = [y_1, \ldots, y_n, y_{n+1}, \ldots, y_{m+n}] = [\sigma(\hat{x}_1), \ldots, \sigma(\hat{x}_n), u_1, \ldots, u_m] \in \mathbf{R}^{n+m}$ is a vector of both the network state $\hat{x}$ and the input u, where $\sigma(\cdot)$ is the nonlinear activation function (e.g., a sigmoid function $\sigma(x) = 1/(1+e^{-x})$). A is a diagonal coefficient matrix, i.e., $A = diag\{-a_1, \ldots, -a_n\} \in \mathbf{R}^{n\times n}$ with $a_i > 0, i = 1, \ldots, n$, and $\Theta = [\theta_1, \ldots, \theta_n] \in \mathbf{R}^{(m+n)\times n}$ with $\theta_i = b_i[w_{i1}, \ldots, w_{i(m+n)}]$, $i = 1, \ldots, n$. w_{ij} is the weight connecting the jth input to the ith neuron where $i = 1, \ldots, n$ and $j = 1, \ldots, (m+n)$. To simplify the discussion, the bias term is not included in the notation as it can be considered an additional constant input, and thus, does not affect the formulation of RNN of Eq. (3). Additionally, it is noted that the RNN model of Eq. (3) is an input-affine system, and therefore, it can be written in the form that is similar to Eq. (1):

$$\dot{x} = \hat{f}(x) + \hat{g}(x)u \tag{4}$$

where $\hat{f}(\cdot)$ and $\hat{g}(\cdot)$ can be derived from the coefficient matrices A and Θ in Eq. (3) and are assumed to be sufficiently smooth. The development of an RNN model follows the two steps (data collection and training process) as discussed in Wu et al. (2019c). Additionally, to ensure that the RNN model of Eq. (3) has the same steady-state as the nonlinear system of Eq. (1), during the training process, the modeling error ν is required to be bounded by $|\nu| = |F(x,u,0) - F_{nn}(x,u)| \leq \gamma|x| \leq \nu_m$, $\gamma > 0$, where $\nu_m > 0$ is the upper bound within the operating region. Similarly, we assume that there exists a control Lyapunov function V and a stabilizing controller $u = \Phi_{nn}(x) \in U$ that renders the origin of the RNN system of Eq. (3) asymptotically stable.

Remark 1. It should be noted that to simplify the discussion, the RNN model of Eq. (3) is formulated as a one-hidden-layer RNN with n states to approximate the nonlinear system of n first-order ODEs of Eq. (1). However, the development of RNN models for approximation of the nonlinear system of Eq. (1) is not restricted to n-state, one-hidden-layer RNN model. Instead, to achieve a desired approximation performance of the nonlinear system of Eq. (1), a multi-layer RNN with a sufficient number of neurons is generally utilized. In that case, the RNN states $\hat{x} \in \mathbf{R}^n$ in Eq. (3) will be the last hidden layer or the output layer of an RNN.

2.5. *Stabilization and safety via control Lyapunov–barrier function*

Control Lyapunov–barrier function (CLBF) has been utilized in Romdlony and Jayawardhana (2016), Wu et al. (2019a) to design a stabilizing controller that drives the state of the nonlinear system of Eq. (1) to the origin while avoiding the unsafe region in state-space. The definition of constrained CLBFs that are designed for the RNN system of Eq. (3) subject to input constraints is as follows:

$$W_c(x) > \rho, \quad \forall x \in \mathcal{D} \subset \phi_{uc} \tag{5a}$$

$$L_{\hat{f}}W_c(x) < 0, \quad \forall x \in \{z \in \phi_{uc}\backslash(\mathcal{D} \cup \{0\} \cup \mathcal{X}_e) | L_{\hat{g}}W_c(z) = 0\} \tag{5b}$$

$$\mathcal{U}_\rho := \{x \in \phi_{uc} | W_c(x) \leq \rho\} \neq \emptyset \tag{5c}$$

where $\rho \in \mathbf{R}$, and $\mathcal{X}_e := \{x \in \phi_{uc}\backslash(\mathcal{D} \cup \{0\}) | \partial W_c(x)/\partial x = 0\}$ is a set of states for the RNN model of Eq. (4) where $L_{\hat{f}}W_c(x) = 0$ (for $x \neq 0$) due to $\partial W_c(x)/\partial x = 0$. $\hat{f}$ and $\hat{g}$ are from the RNN model in the form of Eq. (4).The construction method of the constrained CLBF of Eq. (5) can be found in Romdlony and Jayawardhana (2016) and Wu et al. (2019a), in which a control Lyapunov function and a control barrier function are designed separately and combined together through weighted average.

A feedback control law $u = \Phi_{nn}(x) \in U$ that renders the origin exponentially stable within an open neighborhood ϕ_{uc} that includes the origin in its interior is assumed to exist for the RNN system of Eq. (3) (also in the form of Eq. (4)) in the sense that there exists a $\mathcal{C}^1$ constrained control Lyapunov–barrier function $W_c(x)$ that has a minimum at the origin and satisfies the following inequalities $\forall x \in \phi_{uc}$:

$$\hat{c}_1|x|^2 \leq W_c(x) - \rho_0 \leq \hat{c}_2|x|^2, \tag{6a}$$

$$\frac{\partial W_c(x)}{\partial x} F_{nn}(x, \Phi_{nn}(x)) \leq -\hat{c}_3|x|^2, \forall x \in \phi_{uc}\backslash\mathcal{B}_\delta(x_e) \tag{6b}$$

$$\left|\frac{\partial W_c(x)}{\partial x}\right| \leq \hat{c}_4|x| \tag{6c}$$

where $\hat{c}_j(\cdot)$, $j = 1, 2, 3, 4$ are positive real numbers, $W_c(0) = \rho_0$ is the global minimum value of $W_c(x)$ in ϕ_{uc}, and $\mathcal{B}_\delta(x_e)$ is a small neighborhood around $x_e \in \mathcal{X}_e$. $F_{nn}(x,u)$ is the RNN system of Eq. (3). The universal Sontag controller Lin and Sontag (1991) with $W_c(x)$ replacing the Lyapunov function $V(x)$ can be used as a stabilizing control law $\Phi_{nn}(x)$ that satisfies the conditions in Eq. (6). Additionally, by continuity and the smoothness assumed for f, g and h in the nonlinear system of Eq. (1), there exist positive constants M, L_x, L_w, L'_x, L'_w such that the following inequalities hold for all $x, x' \in \mathcal{U}_\rho$, $u \in U$, and $w \in W$:

$$|F(x,u,w)| \leq M \tag{7a}$$

$$|F(x,u,w) - F(x',u,0)| \leq L_x|x - x'| + L_w|w| \tag{7b}$$

$$\left|\frac{\partial W_c(x)}{\partial x}F(x,u,w) - \frac{\partial W_c(x')}{\partial x}F(x',u,0)\right| \leq L'_x|x - x'| + | \leq L'_w|w_m| \tag{7c}$$

The following theorem is established to demonstrate that in the presence of an unsafe region $\mathcal{D}$, closed-loop stability and operational safety are achieved simultaneously for the RNN system of Eq. (3) under the CLBF-based controller.

Theorem 1. *Consider that a constrained CLBF $W_c(x) : \mathbf{R}^n \to \mathbf{R}$ that has a minimum at the origin and meets the conditions of Eq. (5),exists for the RNN system of Eq. (3). The controller $u = \Phi_{nn}(x) \in U$ that satisfies Eq. (6) guarantees that the closed-loop state stays in $\mathcal{U}_\rho$ and avoids the unsafe region $\mathcal{D}$ for all times for any $x_0 \in \mathcal{U}_\rho$. Additionally, in the presence of an unbounded unsafe region, the origin can be rendered exponentially stable under $u = \Phi_{nn}(x) \in U$, for all $x_0 \in \mathcal{U}_\rho$, while discontinuous control actions $u = \bar{u}(x) \in U$ are required at stationary points x_e ($x_e \neq 0$) for a bounded unsafe region in state-space within $\mathcal{U}_\rho$.*

Proof. It is noted in Wu et al. (2019a) that the unsafe regions $\mathcal{D}$ can be categorized as bounded unsafe regions (e.g., a set of unsafe operating conditions in a chemical reactor) and unbounded unsafe regions (e.g., obstacle avoidance in motion

planning). Specifically, it is pointed out in Wu et al. (2019a) that in the case of an unbounded unsafe region, the origin (i.e., the steady-state of the nonlinear system of Eq. (1)) is the unique stationary point in state-space, and therefore, closed-loop stability and process operational safety can be readily derived under the controller $u = \Phi_{nn}(x) \in U$. However, in the presence of a bounded unsafe region, there exist stationary points (other than the origin) in state-space (i.e., $\mathcal{X}_e$ in Eq. (5b)), and therefore, the stationary points need to be designed to be saddle points and discontinuous control actions will be applied at saddle points to drive the state away from them in the direction of decreasing $W_c(x)$ to ensure closed-loop stability and safety. The detailed proofs for both bounded and unbounded unsafe regions follow closely to those for Theorems 1 and 2 in Wu and Christofides (2019a), and are omitted here. □

3. Real-time CLBF-based predictive controllers using RNNs

In this section, we first present the formulation of CLBF-based predictive controllers using an RNN model and demonstrate that closed-loop stability and safety can be achieved simultaneously for the nominal system of Eq. (1) (i.e., $w(t) \equiv 0$). Subsequently, online learning of RNN models is employed within CLBF-based predictive controllers via the event-triggered and the error-triggered mechanisms to improve RNN prediction accuracy for the uncertain system with time-varying disturbances $w(t)$.

3.1. Formulation of RNN-based CLBF-MPC

Based on the formulation of CLBF-MPC in Wu et al. (2019a), the CLBF-MPC using an RNN model is represented by the following optimization problem:

$$\mathcal{J} = \min_{u \in S(\Delta)} \int_{t_k}^{t_{k+N}} L(\tilde{x}(t), u(t))dt \tag{8a}$$

$$\text{s.t.} \quad \dot{\tilde{x}}(t) = F_{nn}(\tilde{x}(t), u(t)) \tag{8b}$$

$$\tilde{x}(t_k) = x(t_k) \tag{8c}$$

$$u(t) \in U, \quad \forall t \in [t_k, t_{k+N}) \tag{8d}$$

$$\dot{W}_c(x(t_k), u(t_k)) \leq \dot{W}_c(x(t_k), \Phi_{nn}(t_k)) \quad \text{if} \quad W_c(x(t_k)) > \rho_{nn} \quad \text{and} \quad x(t_k) \notin \mathcal{B}_\delta(x_e) \tag{8e}$$

$$W_c(\tilde{x}(t)) \leq \rho_{nn}, \quad \forall t \in [t_k, t_{k+N}), \quad \text{if} \quad W_c(x(t_k)) \leq \rho_{nn} \tag{8f}$$

$$W_c(\tilde{x}(t)) < W_c(x(t_k)) - f_e(t - t_k), \forall t \in (t_k, t_{k+N}), \quad \text{if} \quad x(t_k) \in \mathcal{B}_\delta(x_e) \tag{8g}$$

where $\tilde{x}(t)$, $S(\Delta)$ and N are the predicted state trajectory, the set of piecewise constant functions with period Δ, and the number of sampling periods in the prediction horizon, respectively. The cost function $L(\tilde{x}(t), u(t))$ is generally in a quadratic form that has the minimum value at the equilibrium of the system of Eq. (1) (e.g., $|\tilde{x}(t)|^2_{Q_L} + |u(t)|^2_{R_L}$, where Q_L and R_L are positive definite matrices). The RNN model of Eq. (3) is utilized to predict states $\tilde{x}(t)$ over $t \in [t_k, t_{k+N})$. The objective function of Eq. (8a) is the time integral of $L(\tilde{x}(t), u(t))$ over the prediction horizon. The input constraints of Eq. (8d) are applied over the entire prediction horizon. The state measurement of Eq. (8c) at $t = t_k$ is taken as the initial condition for the RNN models of Eq. (8b). The constraint of Eq. (8e) forces $W_c(\tilde{x})$ along the predicted state trajectories to decrease at least at the rate under the CLBF-based controller $u = \Phi_{nn}(x) \in U$ when $W_c(x(t_k)) > \rho_{nn}$ and $x(t_k) \notin \mathcal{B}_\delta(x_e)$. If $W_c(x(t_k)) \leq \rho_{nn}$, the constraint of Eq. (8f) is activated to maintain the predicted state of the RNN system within $\mathcal{U}_{\rho_{nn}}$ such that the closed-loop state of the nonlinear system of Eq. (1) is bounded $\mathcal{U}_{\rho_{\min}}$. Additionally, if $x(t_k) \in \mathcal{B}_\delta(x_e)$, the constraint of Eq. (8g) decreases $W_c(x)$ over the prediction horizon such that the state can escape from saddle points x_e within finite sampling steps, where $f_e(t)$ is a function that represents the difference between predicted value of $W_c(\tilde{x})$ and actual value of $W_c(x)$ due to a nonzero modeling error. The state measurements of the closed-loop system of Eq. (1) are assumed to be available at each sampling time. The CLBF-MPC optimization problem of Eq. (8) calculates an optimal input sequence but only sends the first control action to the control actuators to be applied over the next sampling period. The theorem below demonstrates that under the CLBF-MPC of Eq. (8), closed-loop stability and process operational safety are achieved simultaneously for the nominal system of Eq. (1) (i.e., $w(t) \equiv 0$) in the sense that the closed-loop state is bounded in the safe operating region $\mathcal{U}_\rho$ for all times, and is ultimately bounded in a small neighborhood $\mathcal{U}_{\rho_{\min}}$ around the origin.

Theorem 2. *Consider the nominal system of Eq. (1) (i.e., $w(t) \equiv 0$) with a constrained CLBF W_c that satisfies Eq. (5) and has a minimum at the origin. Given any initial state $x_0 \in \mathcal{U}_\rho$, it is guaranteed that the CLBF-MPC optimization problem of Eq. (8) can be solved with recursive feasibility for all times. Additionally, under the sample-and-hold implementation of CLBF-MPC based on an RNN model that satisfies the modeling error constraint: $|\nu| = |F(x, u, 0) - F_{nn}(x, u)| \leq \gamma|x| \leq \nu_m$, it is guaranteed that for any $x_0 \in \mathcal{U}_\rho$, the state is bounded in $\mathcal{U}_\rho$, $\forall t \geq 0$, and ultimately converges to $\mathcal{U}_{\rho_{\min}}$ as $t \to \infty$.*

Proof. The proof follows closely to that for Theorem 3 in Wu and Christofides (2019a), and is omitted here. □

3.2. Formulation of RNN-based CLBF-EMPC

The CLBF-EMPC using an RNN model is developed to optimize process economic performance while maintaining the closed-loop state in the safe stability region for all times. The RNN-based CLBF-EMPC is represented by the following optimization problem (Wu and Christofides, 2019b):

$$\mathcal{J} = \max_{u \in S(\Delta)} \int_{t_k}^{t_{k+N}} l_e(\tilde{x}(t), u(t))dt \tag{9a}$$

$$\text{s.t.} \quad \dot{\tilde{x}}(t) = F_{nn}(\tilde{x}(t), u(t)) \tag{9b}$$

$$\tilde{x}(t_k) = x(t_k) \tag{9c}$$

$$u(t) \in U, \quad \forall t \in [t_k, t_{k+N}) \tag{9d}$$

$$W_c(\tilde{x}(t)) \leq \rho_e, \quad \forall t \in [t_k, t_{k+N}), \quad \text{if} \quad W_c(x(t_k)) \leq \rho_e \tag{9e}$$

$$\dot{W}_c(x(t_k), u(t_k)) \leq \dot{W}_c(x(t_k), \Phi_{nn}(t_k)) \quad \text{if} \quad W_c(x(t_k)) > \rho_e \tag{9f}$$

where the notations follow those in the CLBF-MPC of Eq. (8). The CLBF-EMPC optimization problem of Eq. (9) maximizes the time-integral of the objective function $l_e(x, u)$ that represents the process economic benefits over the prediction horizon accounting for the constraints of Eqs. (9b)–(9f). Specifically, the constraints of Eqs. (9b)–(9f) are the same as those for the CLBF-MPC of Eq. (8). The constraint of Eq. (9e) maintains the predicted states within $\mathcal{U}_{\rho_e}$ if the current state $x(t_k) \in \mathcal{U}_{\rho_e}$ at $t = t_k$. However, if the current state leaves $\mathcal{U}_{\rho_e}$, the constraint of Eq. (9f) is activated to drive the state towards the origin such that it can enter $\mathcal{U}_{\rho_e}$ within finite sampling steps.

The theorem below demonstrates that under the CLBF-EMPC of Eq. (9), closed-loop stability, process operational safety and economic optimality are achieved simultaneously for the nominal system of Eq. (1) (i.e., $w(t) \equiv 0$) in the sense that the closed-loop state is bounded in the safe operating region $\mathcal{U}_\rho$ for all times.

Theorem 3. *Consider the nominal system of Eq. (1) (i.e., $w(t) \equiv 0$) with a constrained CLBF W_c that satisfies Eq. (5) and has a minimum at the origin. Given any initial state $x_0 \in \mathcal{U}_\rho$, it is guaranteed that the sample-and-hold implementation of the CLBF-EMPC of Eq. (9) based on an RNN model that satisfies the modeling error constraint, recursive feasibility is guaranteed for all times. Additionally, it is guaranteed that for any $x_0 \in \mathcal{U}_\rho$, the state is bounded in $\mathcal{U}_\rho$, $\forall t \geq 0$.*

Proof. The proof follows closely to that for Theorem 2 in Wu and Christofides (2019b), and is omitted here. □

Remark 2. It is noted that neural networks can also be developed to approximate MPC in a closed-loop system. However, the neural networks that are developed to approximate a regular MPC for closed-loop stability only cannot be directly applied to the problem of operational safety since the controller does not account for operational safety in terms of the avoidance of unsafe sets in state-space. Therefore, to ensure process operational safety, the neural networks that are designed to replace MPC in a closed-loop system should be developed with a training dataset that is constructed using extensive closed-loop simulations under a CLBF-based MPC such that the neural networks are able to learn the optimal solutions (i.e., control actions) that drive the state to its steady-state while avoiding the unsafe region for all times.

Remark 3. In this work, the boundedness of the unsafe sets does not affect the neural network model construction because the RNN model is developed using a dataset with time-series state trajectories that are generated from extensive open-loop simulations within the entire operating region including both safe and unsafe regions. It is noted that the process data from unsafe operation should be used in the development of RNN models because the nonlinear dynamics needs to be well captured in the unsafe region to ensure that the RNN prediction will avoid the unsafe region under the CLBF-based constraints.

3.3. *Online learning of RNNs*

Now we consider the nonlinear system of Eq. (1) subject to bounded time-varying disturbances (i.e., $|w(t)| \leq w_m$) that cannot be fully eliminated by the sample-and-hold implementation of CLBF-based predictive controllers using the RNN models that are developed for the nominal system of Eq. (1) (i.e., $w(t) \equiv 0$). In this case, it is readily shown that the closed-loop system of Eq. (1) may be rendered unstable under the CLBF-based predictive controllers using the initial RNN model for all times since the modeling error between the initial RNN model and the uncertain system of Eq. (1) does not satisfy the constraint $|\nu| = |F(x, u, 0) - F_{nn}(x, u)| \leq \gamma|x| \leq \nu_m$ any more. Additionally, it is noted that the time-varying disturbances $w(t)$ needs to be constrained by a positive upper bound, i.e., $|w(t)| \leq w_m$, $w_m > 0$, to ensure that the closed-loop state can be maintained in the stability region for all times under CLBF-MPC.

To account for the impact of disturbances in the predictions of the CLBF-MPC of Eq. (8) and of the CLBF-EMPC of Eq. (9), the RNN models of Eq. (8b) and of Eq. (9b) need to be updated via online learning using the most recent data to capture the nonlinear dynamics of the system of Eq. (1) subject to the time-varying disturbances $w(t)$. Specifically, in this work, the event-triggered and the error-triggered mechanisms are utilized to implement online learning of RNN models (Wu et al., 2019b). It is noted that the present work focuses on the implementation of online learning of RNN models within CLBF-MPC to ensure both closed-loop stability and operational safety, while the recent work Wu et al. (2019b) addressed closed-loop stability under RNN-based MPC only and does not consider operational safety in the sense of avoidance of unsafe sets.

The event-triggered mechanism updates the RNN model if the following inequality is violated for any $x \in \mathcal{U}_\rho \backslash \mathcal{U}_{\rho_w}$:

$$W_c(x(t)) \leq W_c(x(t_k)) - \epsilon_w (t - t_k), t \in [t_k, t_{k+1}) \tag{10}$$

where $\epsilon_w > 0$. $\mathcal{U}_{\rho_w}$ with $\rho_w < \rho$ is characterized to be the largest level set of $W_c(x)$ within $\mathcal{U}_\rho$ such that if the current state is in $\mathcal{U}_{\rho_w}$, the value of $W_c(x)$ does not increase under the stabilizing controller $u = \Phi_{nn}(x)$ within one sampling period in the presence of bounded disturbances $|w(t)| \leq w_m$, i.e., $W_c(x(t)) < W_c(x(t_k))$, $\forall t \in [t_k, t_{k+1})$. Additionally, it also ensures that the closed-loop state is bounded in $\mathcal{U}_\rho$ and ultimately enters $\mathcal{U}_{\rho_w}$ for any initial state in $\mathcal{U}_\rho$. Detailed proof of the boundedness of state in $\mathcal{U}_\rho$ can be found in Wu et al. (2019b). From Eq. (10), it is shown that the event-triggered mechanism activates the online update of RNN models if the decreasing rate of CLBF $W_c(x)$ is not satisfied within one sampling period. As a result, the RNN prediction accuracy is improved once the online learning is activated using the most recent process data and the closed-loop state can be driven into $\mathcal{U}_{\rho_w}$ at a faster rate.

In addition to the event-triggered mechanism, the following moving horizon error metric $E_{rnn}(t_k)$ is developed to indicate the RNN model prediction accuracy at $t = t_k$:

$$E_{rnn}(t_k) = \sum_{i=0}^{N_b} \frac{|x_p(t_{k-i}) - x(t_{k-i})|}{|x(t_{k-i})| + \delta} \tag{11}$$

where N_b is the number of sampling periods before t_k that contribute to the quantification of the prediction error. $x_p(t_{k-i})$ and $x(t_{k-i})$, $i = 0, \ldots, N_b$ are the predictions of the past states using RNN models, and the past state measurements from the actual nonlinear system of Eq. (1) under the same control actions, respectively. δ is a small positive real number that is introduced in the denominator of Eq. (11) to avoid the division by small numbers when $x(t_{k-i})$ approaches zero. The RNN

model of Eq. (8b) is updated if the accumulated error $E_{rnn}(t_k)$ exceeds the threshold E_T:

$$E_{rnn}(t_k) > E_T \tag{12}$$

where E_T is determined via extensive closed-loop simulations. It should be noted that when an online learning of RNN models is activated, all the data points since the last model update will be used as the training and validation data for the new RNN model. As the number of available data points has a great impact on the RNN model accuracy, N_b and E_T need to be carefully chosen to achieve a desired training performance. Specifically, the moving horizon length N_b is first determined via extensive closed-loop simulations to ensure that there are enough data points that can be utilized in the online update of RNN models, and meanwhile, will not cause data-storage burden. Subsequently, the threshold E_T is determined via simulations off-line to trigger an RNN model update when the state error has accumulated to an undesired level while accounting for common measurement noise, which is sufficiently small compared to time-varying disturbances from model uncertainty, and should not trigger an update of RNN models in most times. Additionally, when the state approaches the unsafe region, the threshold E_T should be adjusted to update online learning more frequently such that the new RNN models are able to capture the most recent dynamics subject to disturbances in a timely manner, and therefore, provide a sufficiently accurate prediction for the CLBF-MPC of Eq. (8) and the CLBF-EMPC of Eq. (9) to avoid the unsafe region. Lastly, after the RNN model is updated at a certain sampling step $t = t_k$, all the errors before $t = t_k$ are reset to zero.

Remark 4. It is noted that the event-triggered mechanism and the error-triggered mechanism may be activated when the conditions of Eq. (10) is violated or the prediction error of Eq. (12) exceeds its threshold at a time instant $t = r_k$ that is within one sampling period, i.e., $r_k \in [t_k, t_{k+1})$. However, since the CLBF-MPC of Eq. (8) and the CLBF-EMPC of Eq. (9) are implemented in a sample-and-hold fashion where the control actions remain the same for each sampling period Δ, i.e., $u = u(t_k)$, $\forall t \in [t_k, t_{k+1})$, the control actions will not be updated immediately after the RNN model update is triggered within one sampling period. In other words, if the online update of RNN models is triggered at $t = r_k \in [t_k, t_{k+1})$, the control actions will still be calculated at the next sampling time, i.e., $t = t_{k+1}$, using the updated RNN models. The asynchronization between the online learning of RNN models and the calculation of control actions using the new RNN models ensures that the sample-and-hold implementations of the CLBF-MPC of Eq. (8) and of the CLBF-EMPC of Eq. (9) remain unchanged, and also leaves enough computation time for RNN models to be updated using the most recent process data.

Remark 5. The main objective of triggered model update is to improve the prediction accuracy of RNN models such that they are able to capture the most recent process dynamics subject to time-varying disturbances. Since the event-triggered mechanism updates RNN models only if the condition is violated, it is demonstrated that the event-triggered mechanism updates RNN models less frequently, and therefore, achieves better approximation performance due to more data available than the regular model update that is triggered every sampling period. Additionally, the frequency of online update depends on the threshold E_T. As a result, the optimal value of E_T is determined via extensive closed-loop simulations to achieve the desired closed-loop performance under disturbances.

Remark 6. In addition to RNN models, the above real-time model update approach can also be applied to linear input/output empirical models. Similarly, we will use the most recent process data to update the parameters in linear input/output empirical models to capture the process dynamics subject to time-varying disturbances. If the modeling error is sufficiently small, then closed-loop stability and operational safety can still be guaranteed under the linear input/output empirical models.

3.4. *Implementation strategy for online RNN learning within MPC*

Based on the event-triggered and the error-triggered schemes proposed in the previous section, the implementation of online RNN learning is integrated with the machine-learning-based CLBF-MPC of Eq. (8) as follows:

Step 1: An initial RNN model that will be utilized in the CLBF-MPC of Eq. (8) is derived from extensive open-loop simulations for the nominal system of Eq. (1) (i.e., $w(t) \equiv 0$) following the construction method in Wu et al. (2019c).

Step 2: Starting from an initial condition $x_0 \in \mathcal{U}_\rho$, the nonlinear system of Eq. (1) is operated under CLBF-MPC in a sample-and-hold fashion with states being continuously monitored and collected. The online update of RNN models is triggered the moment that the decreasing rate of CLBF $W_c(x)$ of Eq. (10) is violated for any $x(t) \in \mathcal{U}_{\rho_w}$, or the moving horizon error detector of Eq. (11) exceeds its threshold E_T for any $x \in \mathcal{U}_{\rho_w}$. At the next sampling time, the new RNN model will replace the old model in the CLBF-MPC of Eq. (8) to solve for the optimal control actions $u^*(t)$ for the next sampling period.

Step 3: When the closed-loop state enters a small neighborhood $\mathcal{U}_{\rho_{\min}}$ around the origin, which is considered to be practically stable for the nominal system of Eq. (1), the error-triggering mechanism is taken off-line until the state leaves $\mathcal{U}_{\rho_{\min}}$ again due to time-varying disturbances.

The online RNN learning within the machine-learning-based CLBF-EMPC of Eq. (9) is implemented similarly to the above strategy for the CLBF-MPC of Eq. (8), and is given as follows:

Step 1: An initial RNN model for the nominal system of Eq. (1) (i.e., $w(t) \equiv 0$) is developed to approximate the nonlinear dynamics in the operating region $\mathcal{U}_\rho$.

Step 2: The nonlinear system of Eq. (1) is operated under CLBF-EMPC in a sample-and-hold fashion and the states are continuously monitored and collected. For any $x(t) \in \mathcal{U}_\rho \backslash \mathcal{U}_{\rho_e}$, where $\mathcal{U}_{\rho_e} \subset \mathcal{U}_{\rho_w}$, the online learning of RNN models is activated following the event-triggered mechanism of Eq. (10). For any $x(t) \in \mathcal{U}_{\rho_e}$, the error-triggered mechanism of Eq. (12) is utilized to adapt the RNN models to the time-varying disturbances using the most recent process data. Similarly, at the next sampling time, the CLBF-EMPC of Eq. (9) will use the updated RNN model to calculate the optimal control actions $u^*(t)$ for the next sampling period.

Remark 7. It is noted that the online learning of RNN models is performed using the most recent process data only by loading the old RNN models with the previous RNN structure and weight matrices as initialization. Therefore, the new RNN models that are trained using new data points inherit

some important features of the nominal process from the old RNN models and also capture the recent dynamics subject to time-varying disturbances from new data points. Additionally, instead of training a new RNN model from scratch, the training process based on the most recent data and the previous RNN model is more computationally tractable, and thus, can be readily incorporated in the real-time implementation of CLBF-MPC.

Remark 8. To ensure that there are enough data points for the online training of RNN models, an additional constraint for the number of collected data points can be employed with the event-triggered and the error-triggered mechanisms without affecting closed-loop stability or safety. Specifically, based on the definition of $\mathcal{U}_{\rho_w}$ as discussed in the section of the event-triggered mechanism of Eq. (10), the closed-loop state is guaranteed to move towards the origin every sampling period (maybe slowly) even if the online learning of RNN models is not activated. Therefore, it allows us to collect enough data points from multiple sampling periods to achieve a better training performance while maintaining the state in the closed-loop stability region. Additionally, in the error-triggered mechanism of Eq. (12), the moving horizon window length N_b for the prediction error of Eq. (11) needs to be carefully chosen to obtain a sufficient number of data points that will be utilized in the online update of RNN models.

Remark 9. Ensemble learning (Sewell, 2010; Mendes-Moreira et al., 2012) and parallel implementation can be utilized to further improve RNN model prediction accuracy for the uncertain systems with time-varying disturbances if the approximation performance of a single RNN model is not desirable. Specifically, as shown in Wu et al. (2019c), multiple RNN models can be developed for the same nonlinear process using different portions of datasets based on a k-fold cross validation, and combined together in the context of ensemble learning to obtain a final prediction result that is superior to a single RNN prediction result. Additionally, parallel implementation of the training processes of multiple RNN models and of the computation of multiple RNN predictions on a high-performance computing cluster can be employed to improve computational efficiency of the real-time CLBF-based predictive controllers in the sense that the computation time for the optimization problem of MPC is rendered less than one sampling period.

Remark 10. It is noted that in this work, we only focus on the implementation of online learning of RNN models within MPC to address operational safety for a fixed unsafe set. However, to handle potential variation of the unsafe set during process operation, real-time process data can be used to re-identify the unsafe sets. As a result, the CLBFs need to be re-designed as well to account for the updated unsafe sets and then be incorporated in CLBF-MPC to achieve simultaneous closed-loop stability and safety.

4. Application to a chemical process example

A chemical process example is provided to illustrate the application of machine-learning-based CLBF-MPC and CLBF-EMPC to operate the system in the safe stability region. Specifically, a well-mixed, non-isothermal continuous stirred tank reactor (CSTR) where an irreversible second-order exothermic reaction takes place is considered. The reaction transforms a reactant A to a product B ($A \rightarrow B$). The inlet concentration of A, the inlet temperature and feed volumetric flow rate of the reactor are C_{A0}, T_0 and F, respectively. The CSTR is equipped with a heating jacket that supplies/removes heat at a rate Q. The CSTR dynamic model is described by the following material and energy balance equations:

$$\frac{dC_A}{dt} = \frac{F}{V}(C_{A0} - C_A) - k_0 e^{-E/RT} C_A^2 \tag{13a}$$

$$\frac{dT}{dt} = \frac{F}{V}(T_0 - T) + \frac{-\Delta H}{\rho_L C_p} k_0 e^{-E/RT} C_A^2 + \frac{Q}{\rho_L C_p V} \tag{13b}$$

where C_A is the concentration of reactant A in the reactor, V is the volume of the reacting liquid in the reactor, T is the temperature of the reactor and Q denotes the heat input rate. The concentration of reactant A in the feed is C_{A0}. The feed temperature and volumetric flow rate are T_0 and F, respectively. The liquid has a constant density of ρ_L and a heat capacity of C_p. ΔH, k_0, E, and R represent the enthalpy of reaction, pre-exponential constant, activation energy, and ideal gas constant, respectively. Process parameter values are listed in Table 1.

Table 1 – Parameter values of the CSTR.

$T_0 = 300\,K$	$F = 5\,m^3/h$
$V = 1\,m^3$	$E = 5 \times 10^4\,kJ/kmol$
$k_0 = 8.46 \times 10^6\,m^3/kmol\,h$	$\Delta H = -1.15 \times 10^4\,kJ/kmol$
$C_p = 0.231\,kJ/kg\,K$	$R = 8.314\,kJ/kmol\,K$
$\rho = 1000\,kg/m^3$	$C_{A0_s} = 4\,kmol/m^3$
$Q_s = 0.0\,kJ/h$	

The CSTR is initially operated at the steady-state $x_s = (C_{As}, T_s) = (1.95\,kmol/m^3, 402\,K)$, and $u_s = (C_{A0_s} Q_s) = (4\,kmol/m^3, 0\,kJ/h)$. The manipulated inputs are the inlet concentration of species A and the heat input rate, which are represented by the deviation variables $\Delta C_{A0} = C_{A0} - C_{A0_s}$, $\Delta Q = Q - Q_s$, respectively. The manipulated inputs are bounded as follows: $|\Delta C_{A0}| \leq 3.5\,kmol/m^3$ and $|\Delta Q| \leq 5 \times 10^5\,kJ/h$. Therefore, the states and the inputs of the closed-loop system are $x^T = [C_A - C_{As} T - T_s]$ and $u^T = [\Delta C_{A0} \Delta Q]$, respectively, such that the equilibrium point of the system is at the origin of the state-space (i.e., $(x_s^*, u_s^*) = (0, 0)$).

The explicit Euler method with an integration time step of $h_c = 2 \times 10^{-5}\,h$ is applied to numerically simulate the dynamic model of Eq. (13). The nonlinear optimization problems of the RNN-based CLBF-MPC of Eq. (8) and of the RNN-based CLBF-EMPC of Eq. (9) are solved using the IPOPT software package (Wächter and Biegler, 2006) and its Python version, named, PyIpopt, with the sampling period $\Delta = 2 \times 10^{-3}\,h$.

We first carry out the closed-loop simulation for the CSTR process of Eq. (13) under the CLBF-MPC of Eq. (8), whose control objective is to operate the CSTR process of Eq. (13) at its steady-state while maintaining the closed-loop state trajectories in the safe stability region $\mathcal{U}_\rho$ for all times. Specifically, we consider an unsafe region $\mathcal{D}$ embedded within the stability region (i.e., a level set of Lyapunov function V) that is defined as an open set, for example, an ellipse described by $\mathcal{D} := \{x \in \mathbf{R}^2 | F(x) = (x_1 + 0.92)^2 + \frac{(x_2 - 42)^2}{500} < 0.06\}$. Following the construction method in Wu et al. (2019a), $\mathcal{H}$ is defined as

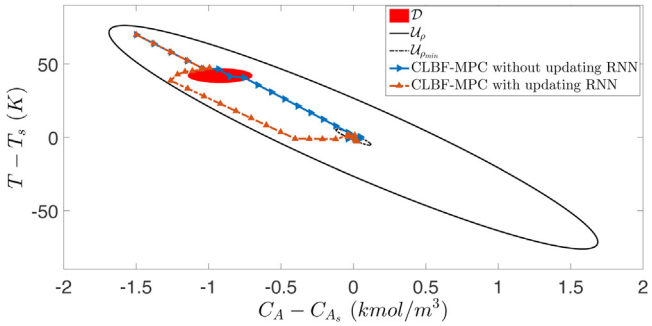

Fig. 1 – The state-space profiles for the closed-loop CSTR subject to time-varying disturbances under the CLBF-MPC of Eq. (8) with (red trajectory) and without online RNN update (blue trajectory), respectively, for an initial condition (−1.5, 70). (For interpretation of the references to color in this figure legend, the reader is referred to the web version of this article.)

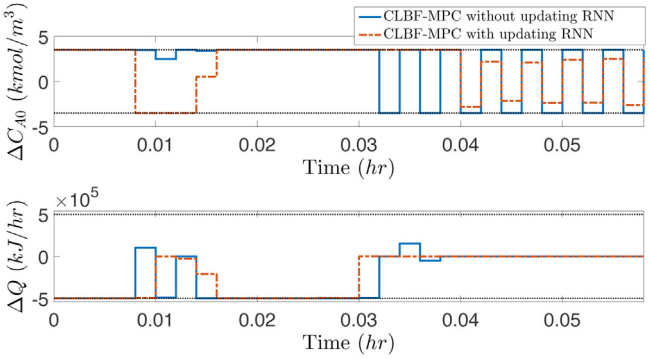

Fig. 2 – Manipulated input profiles ($u_1 = \Delta C_{A0}$, $u_2 = \Delta Q$) for the closed-loop CSTR subject to time-varying disturbances under the CLBF-MPC of Eq. (8) with (red profile) and without online RNN update (blue profile), respectively, for an initial condition (−1.5, 70). (For interpretation of the references to color in this figure legend, the reader is referred to the web version of this article.)

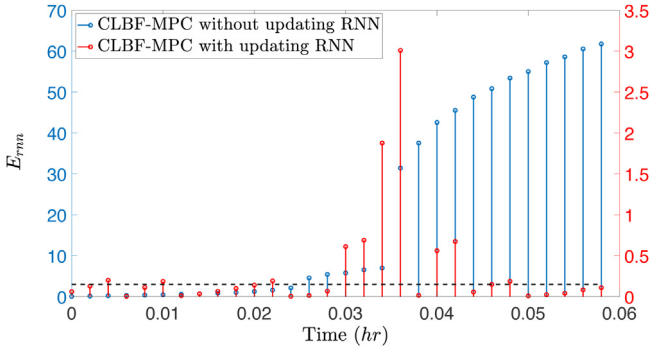

Fig. 3 – Value of $E_{rnn}(t)$ at each sampling time for the closed-loop CSTR subject to time-varying disturbances under the CLBF-MPC of Eq. (8) with (red, right y-axis) and without online RNN update (blue, left y-axis), respectively, where the threshold E_T is set to 0.15. (For interpretation of the references to color in this figure legend, the reader is referred to the web version of this article.)

$\mathcal{H}$:={x ∈ $\mathbf{R}^2$|F(x) ≤ 0.07}, and the control barrier function B(x) is designed as follows:

$$B(x) = \begin{cases} \dfrac{F(x)}{e^{F(x)-0.07}} - e^{-6}, & \text{if } x \in \mathcal{H} \\ -e^{-6}, & \text{if } x \notin \mathcal{H} \end{cases} \tag{14}$$

Additionally, a control Lyapunov function using the standard quadratic form $V(x) = x^T P x$ is constructed with the following positive definite P matrix:

$$P = \begin{bmatrix} 1060 & 22 \\ 22 & 0.52 \end{bmatrix} \tag{15}$$

Therefore, $W_c(x) = V(x) + \mu B(x) + \nu$ is designed with the following parameters $\rho_c = 0$, $c_1 = 0.1$, $c_2 = 1061$, $c_3 = \max_{x \in \partial\mathcal{H}}|x|^2 = 2295$, $c_4 = \min_{x \in \partial\mathcal{D}}|x|^2 = 1370$. $\nu = \rho_c - c_1 c_4 = -160$, and $\mu = 1 \times 10^9$ to meet the conditions of CLBFs in Eq. (5).

Under the CLBF-MPC of Eq. (8), we consider the model variations due to the following disturbances: (1) the feed flow rate F is changing from 5 to 7 m^3/h at t = 0 h, and (2) the actual value of the pre-exponential constant k_0 used in the process model is reduced by half to represent a change in the reaction rate at t = 0 h. The closed-loop simulation results for the CSTR of Eq. (13) under the CLBF-MPC with and without online learning of RNN models, respectively, are shown in Figs. 1–3 . Specifically, in Fig. 1, it is demonstrated that in the presence of disturbances, the closed-loop state trajectory under the CLBF-MPC using online update of RNN models is able to avoid the unsafe region and converge to a small neighborhood around the origin, while the one under the CLBF-MPC without online RNN update crosses the red unsafe region $\mathcal{D}$ due to a considerable model mismatch between the initial RNN model for the nominal process of Eq. (13) and the actual process subject to disturbances. Fig. 2 shows the input profiles under the CLBF-MPC with and without online RNN update, from which recursive feasibility and satisfaction of input constraints are demonstrated for both optimization problems. Additionally, it is observed in Fig. 2 that since RNN models are updated in a timely manner under the CLBF-MPC with online learning, the oscillation of u_1 becomes less near the end of operation period compared to the one without online update.

In the closed-loop simulation, it is demonstrated that the event-triggered mechanism of Eq. (10) is not activated as the closed-loop state moves towards the origin quickly. Therefore, the value of the accumulated prediction errors $E_{rnn}(t)$ of Eq. (11) is shown in Fig. 3 for CLBF-MPCs with and without online RNN update, respectively, to show the real-time prediction accuracy of the RNN models. Fig. 3 demonstrates that without online learning, the error (blue lines) exceeds the threshold (left y-axis) quickly and increases to an undesired level during the operation, which implies the failure of the initial RNN model in capturing the actual CSTR dynamics in the presence of disturbances. However, under the CLBF-MPC with online RNN learning, it is demonstrated that the RNN model update is triggered six times during the entire operation period (i.e., t = 0.06 h) to maintain the error (red lines) below its threshold (right y-axis) for most of the time. Therefore, with online learning, the RNN models used in CLBF-MPC always capture the latest process dynamics subject to disturbances, and lead to a desired closed-loop performance for the CSTR of Eq. (13) in terms of simultaneous closed-loop stability and operational safety.

Subsequently, we carry out the closed-loop simulation for the CSTR of Eq. (13) under the machine-learning-based CLBF-EMPC of Eq. (9) with and without online learning of RNN models, respectively. The disturbance on the feed flow rate F which varies from 5 to 10 m^3/h at t = 0.11 h is introduced into

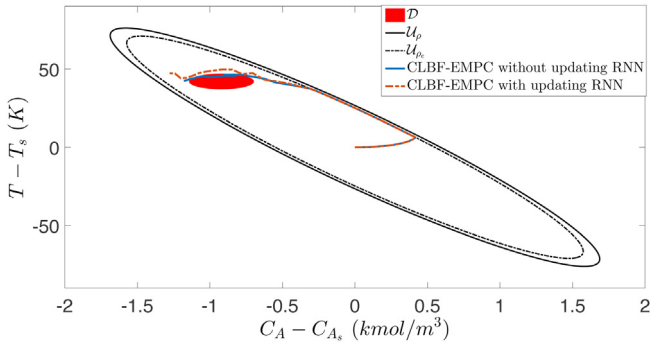

Fig. 4 – The state-space profiles for the closed-loop CSTR subject to time-varying disturbances under the CLBF-EMPC of Eq. (9) with (red trajectory) and without online RNN update (blue trajectory), respectively, for an initial condition (0, 0). (For interpretation of the references to color in this figure legend, the reader is referred to the web version of this article.)

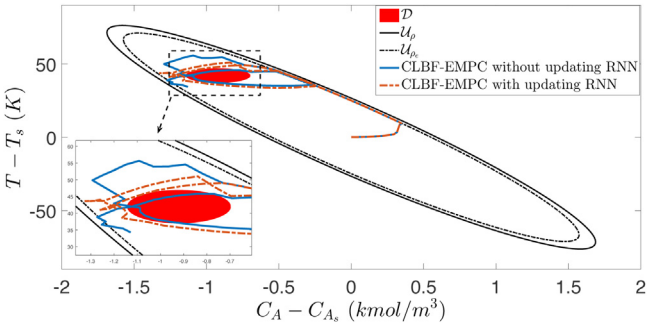

Fig. 5 – The state-space profiles for the closed-loop CSTR subject to time-varying disturbances under the CLBF-EMPC of Eq. (9) with (red trajectory) and without online RNN update (blue trajectory), respectively, for two consecutive operating periods with an initial condition (0, 0). (For interpretation of the references to color in this figure legend, the reader is referred to the web version of this article.)

the closed-loop system. The simulation results are shown in Figs. 4–7 . Specifically, the control objective of CLBF-EMPC is to maximize the profit of the CSTR process of Eq. (13) by manipulating the inlet concentration ΔC_{A0} and the heat input rate ΔQ and meanwhile, maintain the closed-loop state trajectories in the safe stability region $\mathcal{U}_\rho$ for all times. The production rate for the CSTR of Eq. (13)is utilized as the CLBF-EMPC objective function of Eq. (9a):

$$l_e(\tilde{x}, u) = k_0 e^{-E/RT} C_A^2 \tag{16}$$

Additionally, a material constraint is incorporated in the CLBF-EMPC of Eq. (9) to make the averaged reactant material available within one EMPC operating period t_p to be its steady-state value, C_{A0s}. The material constraint is formulated as follows:

$$\frac{1}{t_p}\int_0^{t_p} u_1(\tau)d\tau = 0\,\text{kmol/m}^3 \tag{17}$$

where the averaged reactant material in deviation form, u_1, is equal to 0. In Fig. 4, it is demonstrated that the closed-loop state trajectory under CLBF-EMPC with updating RNN models avoids the unsafe region while the one under the CLBF-EMPC using the initial RNN model for all times enters the unsafe region $\mathcal{D}$ near the end of operating period due to the disturbed feed flow rate F and reaction rate.

Moreover, the closed-loop simulation of the CSTR of Eq. (13) under CLBF-EMPC with multiple operating periods is performed with the following disturbances: (1) the feed flow rate F is changing from 5 to 11.5 m^3/h at $t = 0.1$ h during the first operating period from $t = 0$ h to $t = 0.128$ h, and (2) the actual value of the pre-exponential constant k_0 used in the process model is reduced by 20% to represent a change in the reaction rate at $t = 0.148$ h during the second operating period from $t = 0.128$ h to $t = 0.256$ h. Figs. 5 and 6 show the closed-loop simulation results under the above settings. Specifically, Fig. 5 demonstrates that with online learning of RNN models, the closed-loop state trajectory under CLBF-EMPC is able to avoid the unsafe region for all times within two consecutive EMPC operating periods. Fig. 6 shows the corresponding input profiles under CLBF-EMPC, from which it is observed that the inlet concentration ΔC_{A0} consumes its maximum allowable value at the beginning of each operating period, and thus,

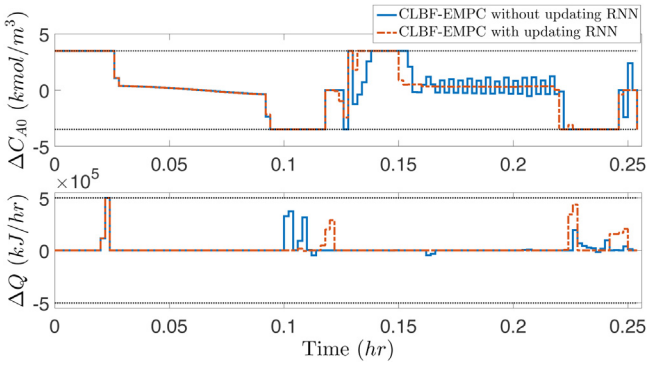

Fig. 6 – Manipulated input profiles ($u_1 = \Delta C_{A0}$, $u_2 = \Delta Q$) for the closed-loop CSTR subject to time-varying disturbances under the CLBF-EMPC of Eq. (9) with (red trajectory) and without online RNN update (blue trajectory), respectively, for two consecutive operating periods with an initial condition (0, 0). (For interpretation of the references to color in this figure legend, the reader is referred to the web version of this article.)

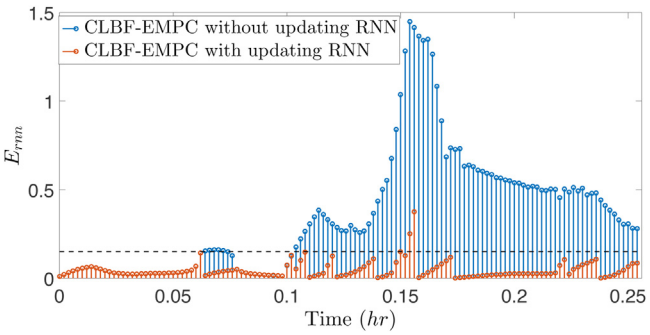

Fig. 7 – Value of $E_{rnn}(t)$ at each sampling time for the closed-loop CSTR subject to time-varying disturbances under the CLBF-EMPC of Eq. (9) with and without online RNN update, respectively, where the threshold E_T is set to 0.15.

decreases to its lower bound near the end of each operating period to meet the material constraint of Eq. (17). Additionally, the accumulated prediction error diagram under CLBF-EMPC with and without online learning of RNN models is shown in Fig. 7. It is demonstrated that the prediction error (red lines) for the CLBF-EMPC with updating RNN models is maintained

at a very low level during the two consecutive EMPC operating periods. However, the prediction error (blue lines) derived from the CLBF-EMPC without updating RNN models indicates a large model mismatch between the initial RNN model for the nominal CSTR of Eq. (13) and the actual disturbed system.

Lastly, to demonstrate the improved process economic benefits under the time-varying operation of EMPC, accumulated economic profits over the entire operating period, i.e., $L_E = \int_0^{t=0.256\,h} l_e(x,u)d\tau$ is compared for the CLBF-EMPC and the steady-state operation (i.e., the CSTR of Eq. (13) is operated at the steady-state for all times). It is obtained that $L_E = 4.93$ for the closed-loop system under CLBF-EMPC with online update of RNN models and $L_E = 2.61$ for the steady-state operation within 0.256 h. Therefore, it is concluded that closed-loop stability, process operational safety and economic optimality are achieved simultaneously for the disturbed CSTR process of Eq. (13) under the CLBF-EMPC of Eq. (9) with online learning of RNN models.

5. Conclusion

In this work, we proposed real-time machine learning-based CLBF-MPC and CLBF-EMPC schemes to optimize process operational safety and closed-loop stability for nonlinear systems subject to time-varying disturbances. The RNN models were first developed for a general class of nonlinear systems and incorporated in the designs of CLBF-MPC and of CLBF-EMPC to provide future state predictions. The event-triggered and the error-triggered mechanisms were then integrated within the real-time implementation of predictive controllers to update RNN models for the uncertain system with time-varying disturbances. The application of real-time machine learning-based predictive controllers to a chemical reactor example demonstrated the benefits of online learning of RNN models in terms of improved closed-loop stability and process operational safety compared to the controllers without online update of RNN models.

Conflict of interest

None declared.

Acknowledgments

Financial support from the National Science Foundation and the Department of Energyis gratefully acknowledged.

References

Ames, A.D., Xu, X., Grizzle, J.W., Tabuada, P., 2016. Control barrier function based quadratic programs for safety critical systems. IEEE Trans. Autom. Control 62, 3861–3876.

Jankovic, M., 2017. Combining control Lyapunov and barrier functions for constrained stabilization of nonlinear systems. In: Proceedings of the American Control Conference, Seattle, Washington, pp. 1916–1922.

Kosmatopoulos, E.B., Polycarpou, M.M., Christodoulou, M.A., Ioannou, P.A., 1995. High-order neural network structures for identification of dynamical systems. IEEE Trans. Neural Netw. 6, 422–431.

Lin, Y., Sontag, E.D., 1991. A universal formula for stabilization with bounded controls. Syst. Control Lett. 16, 393–397.

Liu, D., Yang, G.H., 2018. Neural network-based event-triggered mfac for nonlinear discrete-time processes. Neurocomputing 272, 356–364.

Marquardt, W., 2002. Nonlinear model reduction for optimization based control of transient chemical processes. AIChE Symposium Series, New York; American Institute of Chemical Engineers; 1998, 12–42.

Mendes-Moreira, J., Soares, C., Jorge, A.M., Sousa, J.F.D., 2012. Ensemble approaches for regression: a survey. ACM Comput. Surv. 45, 10.

Romdlony, M.Z., Jayawardhana, B., 2016. Stabilization with guaranteed safety using control Lyapunov–barrier function. Automatica 66, 39–47.

Sahoo, A., Xu, H., Jagannathan, S., 2015. Neural network-based event-triggered state feedback control of nonlinear continuous-time systems. IEEE Trans. Neural Netw. Learn. Syst. 27, 497–509.

Sewell, M., 2010. Ensemble Learning. Technical Report. UCL, London.

Sontag, E.D., 1989. A 'universal' construction of Artstein's theorem on nonlinear stabilization. Syst. Control Lett. 13, 117–123.

Trischler, A.P., D'Eleuterio, G.M., 2016. Synthesis of recurrent neural networks for dynamical system simulation. Neural Netw. 80, 67–78.

Valappil, J., Georgakis, C., 2000. Systematic estimation of state noise statistics for extended Kalman filters. AIChE J. 46, 292–308.

Wächter, A., Biegler, L.T., 2006. On the implementation of an interior-point filter line-search algorithm for large-scale nonlinear programming. Math. Program. 106, 25–57.

Wang, X., Lemmon, M.D., 2008. Event design in event-triggered feedback control systems. In: Proceedings of the 47th IEEE Conference on Decision and Control, 2105–2110, Cancun, Mexico.

Wong, W., Chee, E., Li, J., Wang, X., 2018. Recurrent neural network-based model predictive control for continuous pharmaceutical manufacturing. Mathematics 6, 242.

Wu, Z., Albalawi, F., Zhang, Z., Zhang, J., Durand, H., Christofides, P.D., 2019a. Control lyapunov–barrier function-based model predictive control of nonlinear systems. Automatica 109, 108508.

Wu, Z., Christofides, P.D., 2019a. Handling bounded and unbounded unsafe sets in control Lyapunov–barrier function-based model predictive control of nonlinear processes. Chem. Eng. Res. Des. 143, 140–149.

Wu, Z., Christofides, P.D., 2019b. Optimizing process economics and operational safety via economic MPC using barrier functions and recurrent neural network models. Chem. Eng. Res. Des. 152, 455–465.

Wu, Z., Rincon, D., Christofides, P.D., 2019b. Real-time adaptive machine-learning-based predictive control of nonlinear processes. Ind. Eng. Chem. Res. (in press).

Wu, Z., Tran, A., Rincon, D., Christofides, P.D., 2019c. Machine learning-based predictive control of nonlinear processes. Part I: Theory. AIChE J. 65, e16729.

You, Y., Nikolaou, M., 1993. Dynamic process modeling with recurrent neural networks. AIChE J. 39, 1654–1667.